Design and prototyping of an inverter for Dahlander motors

Rúben André Soeiro Marques
rubenmarques91@gmail.com

Instituto Superior Técnico, Lisboa, Portugal

April 2016

Abstract

This work is focused on the development of an efficient electric drive to power a three phase induction motor in Dahlander setting, to be used in electric vehicles. This kind of motor does not require a mechanical gearbox to switch speeds because its number of active poles can be switched depending on how the connections are made externally. A functional and low cost prototype was designed and constructed for such electric drive. Having designed the inverter from scratch allows a degree of control, customization and expansion that is not achievable with an off the shelf solution. The inverter is characterized over a number of speeds and loads, its efficiency is determined and it is proven capable of regenerative breaking.
Keywords: induction motor, Dahlander setting, electric vehicle, electronic inverter, regenerative braking

1. Introduction

1.1. Motivation

The most challenging requirement that electric vehicles have to meet is a reasonable autonomy. Hybrid vehicles (fuel+electric) and electrified railways are obvious exceptions. The reason behind this challenge is the lower energy density of batteries when compared with fossil fuels. However, unlike a fuel powered vehicle, an electric vehicle can restore its kinetic energy back into its batteries by regenerative braking and recharge them anywhere using solar panels.

Technologies such as energy storage, solar panels and lightweight structures depend on breakthroughs in the areas of chemistry, materials and industry that will not be targeted in this work. This means the effort must be focused in the power train, as the processes of its development are still within the reach of a master thesis.

This work is centred in the development of an electronic inverter for a pole switching (Dahlander) induction motor that is meant to be used in a fully electric solar train for tourists interested in sight seeing. The prototype of the electronic inverter documented in this thesis has the particularity of being capable of switching the number of active pole pairs of the induction motor using two speed regimes like a gearbox, but without the added complexity and ageing susceptibility of switchable mechanical gears.

1.2. State-of-the-art

The inverter documented in this work is designed mainly with electric vehicles in mind, so the state of the art is presented taking this into account. Many types of motors can be chosen and are indeed used in different electric vehicles.

The DC motor is the easiest to control, and they are known for their ability to achieve high torque at low speeds, having already been used in electric vehicles. However they have a bulky construction, low efficiency and reliability [1] and need regular maintenance due to the presence of brushes that eventually have to be replaced, but not before thousands of hours in working condition if properly set [2]. Furthermore, the commutator that interfaces with them has to be cleaned periodically to avoid accumulation of debris between contacts which may damage the motor by flashover [2].

Some DC electric motors create a constant magnetic field using permanent magnets on the stator and the previously discussed brushed wound rotor. If the magnets are placed in the surface of the rotor and the windings in the stator, brushes become unnecessary because the rotor is not wound. Once an alternating current passes through the stator windings a rotating magnetic field is created, forcing the magnets on the rotor to align with this field, turning the shaft. This is a more reliable and robust motor as it does not need brushes, but because the rotor is not wound, the rotor excitation is fixed by the magnets' magnetic field and power has to be finely controlled in the stator. The majority of neodymium

veins on the planet are located on China that manufacturers about 80% of the world's magnets [3], which makes it difficult for a competitive market to exist and get lower prices. Synchronous motors as these offer the advantage of easy regenerative braking, as the rotor has its magnetic field configuration independent of that created with the stator windings. This may be one of the main reasons to why PMSMs are the most used in EV industry; a master thesis [4] listed EVs produced in 2015 and counted 15 among 22 that use PMSMs for their traction.

The induction motor is the most simple, as it does not need either magnets or brushes, which leads to a longer operating life. Its stator is interchangeable with the previous kind of motor, the difference being in the rotor. Its rotor is composed of a series of bars longitudinal to its surface, all connected to each other at the end.

When a rotating magnetic field passes through the rotor, currents are induced in the bars and the resulting Lorentz forces make the shaft rotate.

For greater efficiency, the magnetic field created in the coils should have values within the linear characteristic of the B-H curve of the nucleus material, if not, there will be losses due to magnetic saturation of the material. Assuming a sinusoidal excitation, the voltage dependent of time is described as

$$u(t) = U \cos \omega t \tag{1}$$

that relates with magnetic flux ϕ by

$$u(t) = N \frac{d\phi}{dt} \tag{2}$$

where **N** is the number of windings that generate the flux. Joining these two last equations, integrating in time and solving in order of the flux:

$$\phi(t) = \frac{U}{N\omega} \sin \omega t \tag{3}$$

The magnetic field is just the flux by unit of area **S** so:

$$B = \frac{\phi}{S} = \frac{U}{SN\omega} \sin \omega t = B_{max} \sin \omega t \tag{4}$$

Which means

$$B_{max} \propto \frac{U}{\omega} \equiv \frac{V}{f} \tag{5}$$

the maximum value of the magnetic field is proportional to the voltage between coil terminals **V** and inversely proportional to the frequency of the excitation **f**. When the induction machine is running as a motor, the speed of the shaft is always smaller than the speed of the rotating magnetic field. Furthermore, the maximum voltage that can be applied to the coils is the DC battery voltage. **f** is gradually increased until the maximum **V** is achieved, after that point, increasing **f** will result in lower magnetic field and consequently torque.

In 1897, Robert Dahlander invented a pole changing motor [5], that had two speeds for the same frequency of excitation, depending on how the motor is connected. The number of pole pairs **p** of a motor relates with synchronous speed $\mathbf{N_{RPM}}$ (the speed of the rotating magnetic field) and rotor speed by the following equation:

$$N_{RPM} = \frac{60 \times f}{p} \tag{6}$$

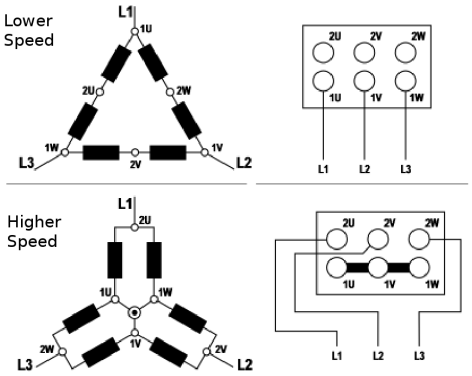

Figure 1: Δ/YY Dahlander configuration connections.

Using an array of relays or a contactor, the connections to the motor can be rearranged while it is running (see Fig. 1) and the operating speed can be extended beyond that allowed by a single number of active pole pairs configuration. The Dahlander setting presents yet another advantage for the project due to a 60% torque increase in demanding scenarios, creating a non-mechanical electrical gearbox of two speeds, lowering weight and removing another mechanical part subject to friction and subsequent ageing. It is important to note that despite the age of this technology and its advantages it is surprising that no reference was found of its use in electric cars.

An electronic inverter provides the pulsed voltage modulation for a pseudo sinusoidal current waveform, allowing a fine control of frequency and current magnitude, resulting in an efficient control of speed and torque. The technologies behind electronic inverters are not particularly new, however the companies that design and build them protect their technology and it is difficult to find documentation on how to properly build one.

1.3. Objectives

The objectives of this work are listed below in the order that they have to be accomplished:

•The characterisation of the induction motor using an autotransformer, therefore with a fixed frequency of 50Hz and varying load. The set of experiments will be done with 1 and 2 active pole pairs.

•Choose the power switching devices (transistors, thyristors, relays, etc) that are more adequate to the demands of the application.

•Design and validate a set of circuits that activate the switching devices.

•Design and validate a voltage sensing circuit to evaluate the state of the battery.

•Design and build a PCB that includes all the needed components for the working inverter.

•Elaborate a control scheme for the inverter-motor set that is capable of switching the number of active poles of the motor and to execute regenerative braking.

•Program the firmware of the microcontroller to reflect the control scheme chosen.

•Characterise the inverter at different speeds and loads, measure its efficiency and iterate along the way to increase its performance regarding efficiency and safety (robustness of the board and code).

2. Induction motor

Two identical induction motors with 2 pole pairs in delta/star setting were rewound into a Dahlander setting of 1-2 pole pairs to be used in the experimentation of the inverter.

The motors' specifications were collected from their nameplate and are represented in Table 1.

Table 1: Relevant information in the motor nameplate

Nr. of phases	3
Setting	Δ/Y
Voltage	220/380 V
Current	4.7/2.7 A
$\cos\phi$	0.8
Power	1.1kW
Frequency	50Hz
Speed	1430 RPM
Design	B

In an electric vehicle that carries passengers it is best to keep voltages low unless all safety measures are taken to avoid electrocution of the occupants or explosion of the battery in accidents. Since the motors have to be rewound into Dahlander setting anyway, a change in the voltage rating can be applied at the same time. The number of turns of each winding are reduced and the cross section of the wires increased for bigger currents, in a way that keeps the amplitude of the magnetic field constant.

Approximating each winding to a long solenoid, the magnetic field B they create when a current I passes through the wires is:

$$B = \mu n I \tag{7}$$

where μ is the medium magnetic permeability and n is the number of turns of the solenoid. Since n is reduced and I is increased in the same proportion, B stays the same. If the number of turns of each winding is reduced to 1/4th of the original, the voltage rating of the motor becomes 1/4th of the original, 55V, which is acceptable.

The open motor revealed that it had 36 slots and 2 sets of windings in each slot, each winding made of 28 turns with a wire cross section of 0.63mm^2. For the reduction to 55V, each winding has to have a new configuration of 7 turns and a wire cross section of 2.52mm^2. A wire this thick is hard to settle in the slots, so the same cross section was used, 0.63mm^2 and each of the 7 turns is in fact a parallel of 4 wires with this cross section.

2.1. Validation of the rewinding process

To validate the rewinding process, the resistance and inductance of the windings of the motors were measured in Δ and YY configurations. The results are represented in Tables 2 and 3 for both motors. 1U-1V-1W and 2U-2V-2W are the points represented in Fig. 1.

Table 2: Resistance and inductance values of the windings of both motors in Δ configuration of 2 active pole pairs

	Motor A		Motor B	
Δ	R(Ω)	L(μH)	R(Ω)	L(μH)
1U-1V	0.44	887	0.26	1360
1U-1W	0.45	882	0.27	1400
1V-1W	0.43	911	0.27	1470
2U-2V	0.45	580	0.27	1340
2U-2W	0.44	592	0.26	1150
2V-2W	0.44	590	0.27	1270
1U-2U	0.32	462	0.17	1450
1U-2V	0.47	473	0.18	656
1U-2W	0.31	910	0.30	813
1V-2U	0.49	476	0.17	821
1V-2V	0.31	931	0.30	821
1V-2W	0.31	496	0.17	1380
1W-2U	0.32	915	0.31	650
1W-2V	0.31	459	0.18	1500
1W-2W	0.47	467	0.18	720

As expected, in Δ configuration the resistance and inductance are very similar between any pair of phases (lines 1,2,3 of Table 2) and between the middle points of the triangle (lines 4,5,6 of Table 2) for both motors. From Fig. 1, lines 1 to 6 of Table 2 correspond to the resistance of 2 series windings in parallel with another 4 series windings. Assuming

Table 3: Resistance and inductance values of the windings of both motors in YY configuration of 1 active pole pairs

	Motor A		Motor B	
YY	R(Ω)	L(μH)	R(Ω)	L(μH)
2U-YY	0.23	249	0.10	386
2V-YY	0.22	250	0.11	390
2W-YY	0.22	247	0.10	411
2U-2V	0.36	335	0.21	851
2U-2W	0.36	339	0.20	886
2V-2W	0.35	342	0.20	922

the 6 windings all have the same resistance value, the measured resistance $R_{2||4}$ depends on the individual winding resistance R by Eq. 8.

$$R_{2||4} = \frac{2R \times 4R}{2R + 4R} = \frac{4}{3}R \tag{8}$$

Which means that for motor A R is 0.33Ω while for motor B R is 0.2Ω.

Lines 7 to 15 of Table 2 correspond either to a parallel of 1 winding with 5 series windings or a parallel of 3 series windings with another 3 series windings. The equations for the expected resistance values are obtained through Eqs. 9 and 10.

$$R_{1||5} = \frac{1R \times 5R}{1R + 5R} = \frac{5}{6}R \tag{9}$$

$$R_{3||3} = \frac{3R \times 3R}{3R + 3R} = \frac{3}{2}R \tag{10}$$

Meaning that the expected resistance values for lines 7 to 15 of motor A are $R_{1||5}$ =0.275Ω and $R_{3||3}$ =0.495Ω. For motor B expected resistance values are $R_{1||5}$ =0.167Ω and $R_{3||3}$ =0.300Ω. While motor B seems to deviate only 10 mΩ from the expected values, motor A is off by as much as 40 mΩ in some measurements.

Lines 1,2,3 of Table 2 show the measurements taken from phase to YY, meaning two windings are put in parallel and the expected resistance of the set is just $R/2$ =0.165Ω for motor A and $R/2$ =0.1Ω for motor B. Lines 4,5,6 are the series of two of these sets, meaning their resistance value is doubled from that of lines 1,2,3. From the results of this last analysis, the resistance values of motor A do not match the expected values. Motor B on the other hand performs perfectly in these perliminary tests.

Motor A did not pass the validation tests and was discarded. Motor B was used in the rest of this work.

2.2. Experimental characterization

It is important to do some measurements of the motor when it is powered with a sinusoidal voltage to be able to compare and evaluate the quality of the electronic inverter. The experimental apparatus consists of induction motor, three phase variable transformer, DC machine, variable DC power source, and power resistors.

Using the three phase variable transformer connected to mains at 50Hz 380V, one can lower the voltage at the motor phases to a chosen voltage value while maintaining the frequency. These tests are undergone in both Δ and YY configuration at the same voltage value 48V, since the Dahlander configuration was designed to be powered by the same power source independently of the number of active pole pairs.

The DC power source powers up the excitation field of the DC machine. The shaft of the induction motor is connected to that of the DC machine and when it rotates, an electromotive force is created at the terminals of the DC machine's armature. If a resistor is connected between such terminals, current can flow, and power can be dissipated.

The efficiency of the set is obtained from the active power consumed by the induction motor and from the power being dissipated on the resistor load.

The active power in Δ and YY is calculated from Eq. 11.

$$P_{elec} = \sqrt{3} V_{RMS} I_{RMS} \cos\phi \tag{11}$$

V being the inter-phase voltage and $\cos\phi$ being 0.8 for this motor, as the nameplate informs (see Table 1).

The power dissipated in the resistor is obtained simply from Eq. 12.

$$P_{load} = VI \tag{12}$$

The efficiency is just the ratio between the last two as shown by Eq. 13.

$$\eta = \frac{P_{load}}{P_{elec}} \tag{13}$$

Efficiency of the set accounts for losses in the induction motor and the generator. Assuming conservatively that the efficiency of the DC generator is approximately 80%, one can obtain a more exact efficiency of the induction motor.

$$\begin{aligned} \eta &= \eta_{ACmot} \times \eta_{DCgen} \\ \eta_{ACmot} &= \frac{1}{0.80} \frac{P_{load}}{P_{elec}} \end{aligned} \tag{14}$$

Finally, one can relate the efficiency of the motor with the slip to find the optimal operating conditions.

Two data sets were obtained for Δ and YY configuration. In Δ the power dissipation and efficiency rise with the opposing torque created by the DC machine. A maximum could not be found in these results because the motor was under-loaded since

no lower load resistance could be put at the terminals of the DC machine and the only way to increase power was increasing speed, which is possible in YY setting. The highest efficiency was achieved at 1435 RPM, with a value of 50.3% and 761.9 W input power. In YY setting the synchronous speed doubled, which allowed higher rotor speed and higher armature voltage in the DC machine, leading to higher dissipated power, torque and efficiency. In this configuration, an efficiency maximum was found at 2813 RPM, corresponding to a slip value of 187 RPM, 71.2% efficiency, 1299.3 W of input power. This slip value is a good indicator to the value that the inverter will have to ensure for the highest efficiency.

The equivalent circuit of the induction motor is depicted in Fig. 2 and its parameters are useful to establish relations between voltage, current, power factor and torque and for advanced control techniques like vector control. Therefore, two tests are executed in a setup very similar to the previous one, with 2 active pole pairs, to extract these parameters.

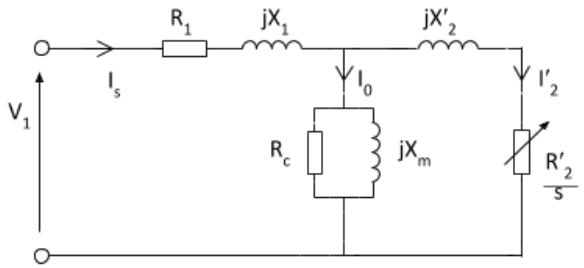

Figure 2: Steinmetz equivalent circuit of the induction motor

One of the tests consists in powering the induction motor with close to nominal voltage between phases and forcing the synchronous speed with the DC motor. Therefore, the slip is zero and the right hand side of Fig. 2 equivalent circuit becomes a high impedance.

This makes it easy to calculate the equivalent core resistance R_c and inductance X_m, assuming that these last two are much greater than the resistance of the stator coils R_1 and stator leakage inductance X_1, which means that that in this case there is approximately no voltage drop over R_1 and X_1. Considering the power factor $\cos\phi$ and the input current in one phase I_S, in this case equal to I_0, one can extrapolate the current that passes in the core resistance I_w and in the core reactance I_m. Regardless of the configuration, I_S is always the phase current of the transformer and the phase voltage V is the phase to neutral voltage of the transformer.

$$I_0 = I_{RMS} \tag{15}$$

$$I_w = I_0 \cos\phi \tag{16}$$

$$I_m = I_0 \sin\phi \tag{17}$$

To obtain $\cos\phi$, one has to use the relation between active and apparent power using Eq. 18.

$$P_{active} = P_{app} \cos\phi \tag{18}$$

$$P_{app}(t) = V(t)I(t) \tag{19}$$

But P_{active} is also the time average of P_{app} over an arbitrary number of periods, so finally:

$$P_{active} =< P_{app} >_t \tag{20}$$

$$\cos\phi = \frac{P_{active}}{P_{app}} \tag{21}$$

Using the assumption of zero voltage drop in R_1 and X_1:

$$R_c = \frac{V}{I_w} \tag{22}$$

$$X_m = \frac{V}{I_m} \tag{23}$$

$$L_m = \frac{X_m}{2\pi f} \tag{24}$$

The other test consists in blocking the rotor by hand and applying a sinusoidal voltage between phases using the autotransformer, in a way that the current does not exceed the nominal value. Since the slip is one, the total rotor resistance seen by the stator R_2' is much lower and R_c and X_m can be neglected.

As previously, using Eqs. 18-21 one can calculate the power factor $\cos\phi$. The relation between $R = R_1 + R_2'$ and $X_L = X_1 + X_2'$ can be calculated from the phase angle ϕ using Eq. 25.

$$\tan\phi = \frac{X_L}{R} \tag{25}$$

The magnitude of the complex impedance $Z = R + X_L$ is represented in Eq. 26.

$$|Z| = \sqrt{R^2 + X_L^2} = \frac{V_{RMS}}{I_{RMS}} \tag{26}$$

Combining Eqs. 25 and 26, R and X_L can be determined.

R_1 represents the resistance of the stator windings of one phase. This was in part already measured in Tables 3 and 3. R_1 is simply the measured resistance value between the phases of motor B in Δ configuration.

R_2' is calculated from the difference of the estimated R value and R_1:

$$R_2' = R - R_1 \tag{27}$$

With X_L determined, X_1 and X_2' can be obtained using the standard relation between stator and rotor inductances in design B motors [6]:

$$\frac{X_1}{X_2'} = 0.67 \tag{28}$$

The parameters obtained from these two tests are summarized in Table 4.

Table 4: Parameters of the induction motor equivalent circuit

R_1	0.267 Ω
R_2'	0.003 Ω
X_1	0.105 Ω
X_2'	0.156 Ω
R_c	17.54 Ω
X_m	1.63 Ω

3. Design and construction of a three phase inverter

A three phase electronic inverter is needed to generate an AC current on each phase, the main part of it being a triple half bridge composed of power semiconductors and whose simplified schematic is shown in Fig. 3

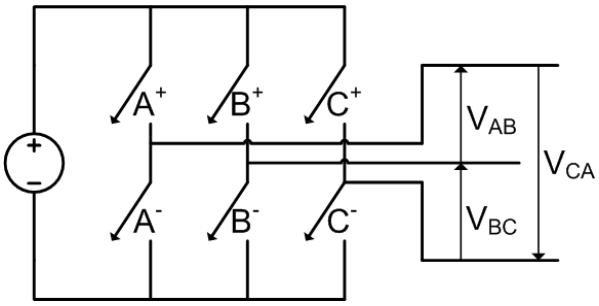

Figure 3: Simplified schematic of a three phase inverter.

One of the first design options is to choose between MOSFET or IGBT technology as the power semiconductors that are at the inverter's core. International Rectifier and Mouser Electronics each released a document about the choices between the two technologies [7][8]. As power requirements and voltage increases IGBT become more addequate as long as the switching frequency stays low, which is the case of this inverter, but a final decision cannot be made without actually testing the efficiencies of both technologies in this application. For the proof of concept MOSFET were used, specifically the FDA75N28 [9], only because the laboratory already had them in stock and they satisfied the requirements.

3.1. Transistor control

These particular transistors turn on when their V_{GS} rise above ∼4V which is imposed by circuits that are superficially explained in the limited extent of this document.

Q2, **Q4** and **Q6** have their Sources on the same net and the control is simpler, as the same voltage referential can be used for the three transistors when applying voltage between Gate and Source. A CD4050 hex non-inverting buffer [10] was used to activate and deactivate the transistors, with PC851 optocouplers [11] physically isolating the low and high power sections of the board. Resistors were chosen based on simulations and experimental samples from the circuit.

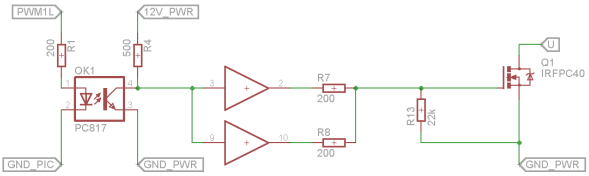

Figure 4: Schematic of the gate driver of one of the bottom transistors including two cd4050 gates and one optocopler circuit.

Q1, **Q3** and **Q5** have Sources on different nets with potentials that change, therefore a virtual ground has to be established with each of them. This is accomplished using the circuit in Fig. 5.

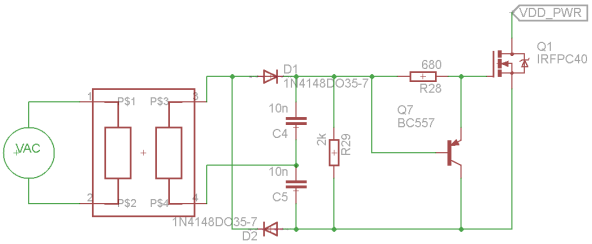

Figure 5: Schematic of the gate driver of one of the top transistors showing the pulse transformer and the voltage doubler rectifier circuit.

Three signal transformers are used to separate grounds, one for each MOSFET. At the same time, these transformers serve as the physical separation between the signal and power areas of the board. An alternating voltage is applied on the primary and a full wave voltage doubler rectifier on the secondary charges the MOSFET gate through a resis-

tor. When the alternating voltage on the primary is removed, capacitors **C4** and **C5** discharge naturally through **R29** and current flows from the gate of **Q1** back into **R28** and **R29**. As the voltage increases at the terminals of **R28**, the voltage between base and emitter of **Q7** makes it conduct some current, discharging the gate and making **Q1** turn off faster.

The AC voltage excitation is achieved with one CD4049 hex inverting buffer for the control of each of the three transistors drives. With an hex inverting buffer, only one of the output pins of the microcontroller is enough to drive both ends of the tranformer's primary if the setup is as depicted in Fig. 6.

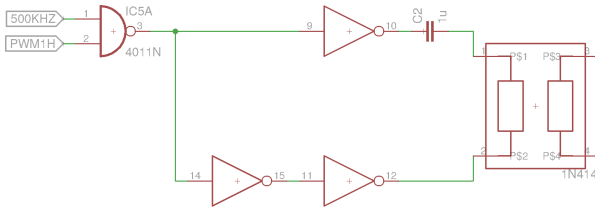

Figure 6: Simplified schematic of the logical not gates that drive the pulse transformer in the gate driver of Fig. 5.

The cd4049 has 6 gates, and if one of these is used for the control of each transistor, 3 unused gates remain. 2 of these gates are used in parallel with the gates actively driving the pulse transformer, with protection resistors much alike the setup of Fig. 4.

When the output of the NAND is logic High, pin 10 of Fig. 6 will be Low and pin 12 High due to double negative. The input will be either a 500kHz excitation that can turn on the MOSFET or a constant voltage that cannot.

3.2. Changing the number of active poles

This particular inverter was designed to be able to change the number of active poles of a Dahlander motor. Fig. 1 already gives a hint on how to implement the hardware for these commutation.

The 3 wires that carry power from the triple half bridge are switched by 3 relays that select their output path, to the 1U-1V-1W motor connections in Δ setting or 2U-2V-2W in YY. A second set of 2 relays manage a short or open circuit between 1U-1V and 1V-1W, effectively short circuiting the three wires in YY. Since all the relays have only two states that have to be switched simultaneously, only one driver is enough to command the whole array, such driver being the ULN2803 [12] conveniently available in the microcontroller development board used in this work.

3.3. Battery level monitor

A voltage level monitor is important to check the remaining charge and protect the battery from discharging below a set point where, while still performing acceptably, greatly reduces the battery's remaining cycles. This set point may be adjusted in the firmware for a tradeoff between autonomy and aging speed of the battery.

An NE555 timer [13] was used as a voltage controlled oscillator (VCO) as the core of the voltage monitor, isolated from the microcontroller using a PC851 optocoupler [11]. As the name suggests, a VCO changes the frequency of the output wave depending on the input voltage. A microcontroller measures this frequency and infers the input voltage.

3.4. Surge protection

Rapidly shifting high currents of ~30A over inductive loads as motor windings creates strong back electromotive forces in the circuit that has to be protected against it. Most power transistors already have freewheeling diodes built-in to mitigate this issue.

This particular application tested switching at 4kHz and 8kHz. When one of the transistors in one of the three half bridge closes, overshoot and ringing are observed between drain and source terminals of the other transistor in the same half bridge due to charge resonating back and forth between the inductance of the winding and the capacitance between drain and source pins.

Overshoot becomes an issue if the resulting voltage is higher than the absolute maximum referenced in the transistor datasheet, in which case the device may fail completely becoming a fire hazard if switching high power.

To tackle this problem, a snubber network as simple as a RC filter in parallel with each transistor can slow the rate at which the V_{DS} changes, so that the voltage overshoot peak value is smaller and the energy that was previously being dissipated in the transistor is now being dissipated in the snubber. Furthermore, adding a schottky diode in parallel also helps, since this is a much faster diode than the body diode of the MOSFET that starts conducting earlier and lowers the overshoot peak. The component dimensioning method that was followed is detailed in the full document. Using the snubbers, an overshoot reduction from 80V to 60V was achieved.

The stability of the 12V power rail is another concern. This inverter is tested with a power source composed of 4×12V batteries. The one connected to ground also powers the CD4050 that controls the lower transistors. If voltage fluctuates too much, the output of the gates becomes ambiguous and in-

correct states may happen. In extreme cases, one branch of the bridge can be shorted and transistors are destroyed. Using an LC filter this issue was mitigated.

An LC filter was also applied in the DC bus for current spike limitation on the battery's end. A relatively big capacitor bank of 8.8mF was used as the main aid to the battery, supplying the immediate current that was required or dumped by the inverter and the battery supplyed the average current. A series of switches were mounted to allow safe charge and discharge of the capacitors with an LED for user convenience that showed the state of the capacitor's charge.

4. Motor control

4.1. Field Oriented Control - Sensorless

Field Oriented Control (FOC) is the most efficient vector control scheme [14] and has been used in the industry since the 1980s, after the commercialization of microcontrollers, to control synchronous and asynchronous machines alike.

FOC is based in a set of transformations of coordinates that effectively lead to a system in which flux and torque can be controlled individually.

The current in two phases is acquired and the third is calculated from the two other since the sum of all is zero. The currents are represented as vectors in a 3 axis referential. A Clark transform is executed to represent these currents in a two axis fixed frame referential.

Next, the current in this new referential is projected by Park transform into a rotating reference frame that "follows" the rotor using an estimation of its position. In this referential, if the current vector is incremented in one axis the flux is incremented, the other axis controlling torque. A control algorithm is executed to control the speed of the motor and the V/f relation. After the references are calculated in this referential, the inverse transformations take place and the voltages applied to the phases are set using some kind of modulation technique such as space vector modulation.

4.2. Sensored control

As an alternative to the more abstract sensorless control, a simpler sensored speed control can be implemented using a custom made tachometer attached to the shaft of the motor so that the microcontroller can keep the ∼180 RPM slip value for highest efficiency.

The modulation is done using a look up table which is easily reconfigured in the microcontroller firmware and indicates the timings of the 6 transistors in one unique pseudo sinusoidal set of on times. Switching frequency can also be reconfigured. As expected, symmetric activation sequences give better results overall with more balanced currents but marginally better efficiencies at 45 % highest, in comparison to other not so well balanced sequences at 42.5 %. Higher commutation frequency is better because the harmonic content of the current is minimized, but the highest frequency is dependent of the hardware limitations such as turn on and off times of the transistors.

A V/f set of slopes is followed by the microcontroller automatically trying to keep slip constant. Another degree of freedom is added by the use of a potentiometer that weakens V by a percentage corresponding to the position of the potentiometer. The upper half of the values indicate how much power is required by the user, the lower half is how much to regenerate, ends corresponding to no attenuation in V.

Whenever the calculated magnetic field rises above 1550 RPM, the relays switch to 1 active pole pair and the frequency is lowered to 25 Hz and incremented from this value. If the speed gets below 1450 in YY setting the relays switch again to 2 active pole pairs.

4.3. Regenerative braking

For regenerative braking to happen, the rotor has to move faster than the rotating magnetic field. This is accomplished using the DC machine as the motor and the induction machine as the generator. The same apparatus described previously in this section is used for these experiments but now the armature of the DC machine is powered by a second DC power supply instead of being connected to load resistors.

The setup was tested with 4kHz symmetric switching, at a speed of 1540 RPM and a slip of -180 RPM. The power consumed by the DC motor to put the machines in motion was 57W. Negative current spikes are observed in this test showing that regenerative braking is indeed happening, but still the average of the current does not invert, meaning that the induction machine is consuming more power from the battery that it is regenerating.

More tests under different conditions are run without success braking regeneratively.

Stefan Schmitt is a german student that worked with this inverter for four months at IST and reworked the firmware to implement FOC as described in the beginning of this Section. Two current probes have been added to the original design to enable this method and the rotor velocity meter was discarded. Apart from these modifications, from the hardware perspective the inverter was not altered.

With FOC it was finally possible to observe regeneration. The results of his work are presented here as proof of the hardware capabilities. The control algorithm follows a very similar approach to the

already described FOC topology.

In one test, the average power being regenerated into the battery was 264W, and the power delivered to the DC machine was 684W, which gives a total efficiency of ∼39% for the experimental setup.

5. Conclusions

A three phase interter was designed taking into account the possible semiconductor technologies available and designing the drive circuits for the chosen technology, MOSFET.

The inverter's PCB was designed in OrCAD Layout 9.2 and printed using an LPKF miller available in the lab. Surge protection circuits were included as modifications to the original board and were included in a new schematic done in the more recent and more user friendly CadSoft EAGLE 7.2.0. PCB design started from scratch due to the program change and is at the time of writing at ∼70 %.

This inverter has the ability of changing the motor's number of active pole pairs switching the connections of the inverter to the motor with an array of relays.

A rudimentary speed control technique was devised, coupled with configurable set points for voltage dependent of frequency. This control could not execute regenerative braking, but it was made possible using FOC.

The experimental apparatus for the testing of the inverter has to be reworked to make the testing of the inverter in lower speeds possible, namely using a higher power DC machine or a lower value load resistance.

5.1. Achievements

The most common types of electric motors were discussed in the scope of an electric vehicle, namely an ultra light solar train, after which the induction motor was chosen.

2 induction motors that were wound in a Δ/Y configuration of 2 pole pairs were rewound offsite for a Dahlander Δ/YY setting of 1 and 2 switchable active pole pairs. The two motors were put through a validation process, after which one of them was discarded for poor performance. The other motor was tested, being found that a slip of 180 RPM corresponded to the point of highest efficiency, giving insight to what slip the inverter had to mimic.

The range of applicability of different types of semiconductor technology was studied in detail, leading to MOSFET being implemented in this inverter.

Common isolated transistor drives use DC-DC converters which in this context are a sort of isolated small power supplies that provide independent virtual grounds for the transistors, but tend to be relatively expensive. An alternative dedicated circuit was developed with discrete components for transistor drive which works properly and has the potential of becoming cheaper than using DC-DC converters.

Snubber circuits and voltage stabilizers were investigated for surge protections in many parts of the circuit, being included most of the times after the printing of the PCB, resulting in many improvisations in the present board and a list of changes in the next iteration.

A prototype of a voltage monitor was designed and tested in a breadboard with a reduced voltage level of 10-15 V, performing correctly but not being yet included in the present version of the inverter.

A custom made tachometer was adapted to the motor so that the microcontroller may have velocity feedback.

A simple control scheme was applied to intuitively use a potentiometer as an accelerator, in a way that the user requires torque instead of speed.

Many types of look up tables were tested at different frequencies. It is only with FOC that regenerative braking can be achieved.

This work provides the flexibility that no other commercially available inverter allows from an academic point of view. Since the work performed in the lab included both the microcontroller's firmware development and the research, choice and assembly of every part in the circuit of the inverter, any kind of customization can be possible. The next iteration of this board can certainly be used in academic lab context to customize different regimes of operation and explain how the inverter itself works deconstructing its complexity.

5.2. Future Work

Despite the working state of the inverter, a new board has to be designed with the improvised modifications applied to the original one. These modifications include the snubbers, the LC filter for the stabilization of the CMOS non-inverting IC and the inclusion of a level shifter IC to avoid the 8.5V mid range voltage level in the board.

A thorough characterization of the inverter performance is still missing, mainly because so much time was invested in repairing the inverter and iterating along the necessary modifications in the hardware and software. Also, since the opposing torque is supplied by a DC machine that dissipates power in resistors, the opposing torque is proportional to the speed unless the excitation voltage becomes higher or the load resistance becomes lower. In the tests that were made, both were at the limit that was available, so the tests were all made at the highest speed that was relevant using 2 active pole pairs, ∼1500 RPM. To test the inverter in lower speeds, the setup has to be changed. The inverter did drive the motor in YY configuration under no-

load, but loaded experiments were not considered until late in the development phase when the inverter was prepared for those. By this time the experiments had already stopped for the elaboration of this document.

The FOC algorithm that was implemented as a proof of concept by Stefan Schmitt has to be documented for future uses.

Since voltage and power will rise if this inverter is used in a real life situation, IGBT may be more adequate that MOSFET, so this offers another degree of freedom and should be investigated.

In a real vehicle the temperature of the motor becomes a concern as does the temperature of the inverter components, since these parts might not be as well ventilated as in a workbench, nor they have a pulsed operation for momentary data acquisition and analysis.

In an electric vehicle with more than one motor, an electric differential is paramount to control the speed of the wheels. Some form of communication between a master controller and the slave inverters has to be used, RS485 being one of the most common options.

References

[1] X. Xue. Selection of electric motor drives for electric vehicles. In *Power Engineering Conference, 2008. AUPEC '08. Australasian Universities*, 2008.

[2] Austin Hughes. *Electric Motors and Drives - Fundamentals, Types and Applications*, chapter 3, page 86. Elsevier, 2006.

[3] Patrice Christmann. The demand for rare earth materials in permanent magnets.

[4] Tomáš Hlinovský. Optimal control of mathematical model of the electrovehicle. Master's thesis, Czech Technical University in Prague, 2015.

[5] Device for varying the number of poles in alternate-current motors.

[6] IEEE Power Engineering Society. *IEEE Standard Test Procedure for Polyphase Induction Motors and Generators*, 1996. IEEE Std 112™-2004.

[7] Carl Blake and Chris Bull. *IGBT or MOSFET: Choose Wisely.* International Rectifier.

[8] Bill Schweber. Basics of mosfets and igbts for motor control. Mouser Electronics.

[9] Fairchild Semiconductor Corporation. *FDA75N28 280V N-Channel MOSFET*, 10 2006.

[10] Fairchild Semiconductor Corporation. *CD4049UBC CD4050BC Hex Inverting Buffer Hex Non-Inverting Buffer*, 10 1987. Rev. 4 2002.

[11] Sharp. *PC851 High Collector-emitter Voltage Type Photocoupler.*

[12] Texas Instruments. *ULN2803A Darlington Transistor Arrays*, 1 2015.

[13] Texas Instruments. *xx555 Precision Timers*, 9 1973. Rev. 9 2014.

[14] Carl Blake and Chris Bull. *Field Orientated Control of 3-Phase AC-Motors.* Texas Instruments, 2 1998. Literature Number: BPRA073.